Spatial Predictor Selection for Next-Day Minimum Temperature Forecasting: An Automated Machine Learning Framework Applied Across European Climate Regimes

Eric Duhamel

Correspondence: edilia12380@gmail.com

This manuscript is a non-peer-reviewed preprint submitted to EarthArXiv.

Abstract

Accurate prediction of daily minimum temperature (Tmin) is critical for frost protection, energy management, and public health preparedness. While numerical weather prediction models have improved substantially, their performance for Tmin forecasting remains limited by difficulties in representing fine-scale nocturnal processes. This study presents an automated framework for identifying optimal spatially-distributed predictors for next-day Tmin forecasting, applied to eight climatically diverse sites across Western Europe.

Using 26 meteorological variables from ERA5 reanalysis data spanning 2004–2024, we systematically explored a search space of approximately 45,000 candidate predictors within a 540 km radius around each target station. An iterative optimization algorithm guided by mean absolute error (MAE) identified 90-predictor configurations for each site. Three regression models—linear regression, LightGBM, and XGBoost—were evaluated, with XGBoost consistently achieving optimal performance.

Results demonstrate substantial skill across all sites, with MAE ranging from 0.81°C (Nice, Mediterranean) to 1.34°C (Brest, oceanic), representing 35–54% improvement over persistence and 51–64% over climatological baselines. The analysis revealed both universal patterns—near-surface air temperature dominated predictive gain at all sites (37–66%)—and distinctive climate-specific signatures: Mediterranean stations exhibited strong persistence signals (30% contribution from previous-day Tmin), oceanic climates showed enhanced dewpoint importance (16%), and continental sites featured significant soil temperature contributions (14%).

Predictor selections proved highly stable at the variable level (23–24 of 26 variables consistently selected across independent runs), while spatial autocorrelation caused greater variability in specific grid-point selections. Importantly, 80% of predictive gain originated from just 4 predictors and 90% from 12 predictors, suggesting that substantially reduced configurations could achieve comparable performance for operational applications.

While the absolute MAE values reflect the idealized nature of reanalysis data and are not directly transferable to operational contexts, the methodology for predictor identification remains valid and applicable to numerical weather prediction outputs. This framework provides a systematic, reproducible approach to spatial predictor selection that can be adapted to other forecasting variables and domains.

Keywords: *minimum temperature forecasting, spatial predictor selection, machine learning, ERA5 reanalysis, gradient boosting, climate-specific signatures, Western Europe*

1. Introduction

1.1 Context and motivation

Forecasting daily minimum temperatures represents a major challenge in operational meteorology with significant implications across numerous sectors. Accurate predictions of the next day's minimum temperature are essential for protecting crops against frost, managing energy demand, winter road maintenance, and preparing public health services during cold spells (Wilks, 2011). Unlike maximum temperature forecasting, minimum temperature prediction is particularly sensitive to nocturnal radiative cooling, local topography, soil moisture conditions, and atmospheric boundary layer stability—factors that exhibit strong spatial variability and complex interactions (Stull, 1988). Numerical weather prediction (NWP) models, although constantly improving, often struggle to capture the fine-scale processes that control minimum temperatures, particularly in complex terrain or coastal areas. This limitation has motivated the development of statistical post-processing methods—often referred to as Model Output Statistics (MOS) (Glahn and Lowry, 1972)—capable of exploiting patterns in historical data to refine NWP model outputs or establish empirical relationships between atmospheric variables and surface temperatures.
The spatial distribution of predictor variables represents a key but often under-explored dimension in temperature forecasting. While most statistical approaches focus on temporal structures or rely solely on local observations, atmospheric processes such as advection, regional cloud cover patterns, and maritime influences suggest that information from surrounding locations could significantly improve forecast quality. However, the optimal spatial configuration of predictors—which variables to use, at what distances, and in which directions from the target site—remains largely site-specific and poorly characterized.

1.2 Research objective and scope

The primary objective of this study is to identify optimal sets of spatially distributed predictors for next-day minimum temperature forecasting at reference sites across Western Europe. It is crucial to emphasize that this work focuses on **predictor selection methodology** rather than achieving the lowest possible prediction error in an operational context.

More specifically, we aim to:

1. Develop and validate an automated framework for systematic spatial exploration and predictor selection
2. Identify which meteorological variables, at what distances and in which directions from target sites, provide the most valuable information for Tmin forecasting
3. Characterize how optimal predictor configurations vary across sites with contrasting climatic characteristics (maritime vs. continental, coastal vs. inland, northern vs. southern)
4. Quantify the added value of spatially distributed predictors compared to purely local approaches

This study uses a one-day temporal window to forecast the minimum temperature one day ahead, drawing on 26 meteorological variables derived from ERA5 reanalysis data (Hersbach et al., 2020) covering Western Europe, in addition to minimum temperature data from reference sites. The latter originate from NCEI-NOAA sources and correspond to actual observations. We apply this methodology to eight reference sites with diverse climatic characteristics (Peel et al., 2007), ranging from Mediterranean coastal sites to inland continental locations.

It should be noted that the choice of minimum temperature as the target variable primarily serves to illustrate the methodological principle. The developed approach is inherently generic and should apply without major difficulty to other meteorological variables (maximum temperature, precipitation, wind, humidity, etc.) or even to non-meteorological domains. For example, one can envisage its application to river gauge level forecasting in hydrology, pollutant concentration forecasting in air quality, or any other environmental variable exhibiting spatio-temporal structure.

1.3 Methodological approach

Our approach combines systematic spatial exploration with machine learning regression techniques (Chen and Guestrin, 2016) (Ke et al., 2017) to automatically identify informative predictor sets. For each reference site, we explore the surrounding geographic space to extract candidate predictors from a set of 26 meteorological variables at different locations. These predictor sets are then evaluated using three complementary regression models—Linear Regression, LightGBM, and XGBoost—with mean absolute error (MAE) serving as the selection criterion.

Mathematical formulation: The regression problem can be expressed as finding the optimal function *f* such that:

$$Tmin_{t+1}=f(X_{1,t},X_{2,t},\ldots,X_{n,t})+\varepsilon_{t+1}$$

where X_i represents each predictor triplet (variable, latitude, longitude) at current day, and ε is the residual error. The objective is to minimize: $MAE = (1/N)\ \Sigma|Tobs - Tpred|$

where T_{obs} and T_{pred} denote the observed and predicted minimum temperatures, respectively, and the summation is taken over the N verification samples.

The use of multiple regression algorithms serves two purposes: (1) ensuring that identified predictors are robust regardless of the modelling approach, from linear to non-linear methods; and (2) providing insights into the nature of relationships between predictors and target temperatures.

To validate the added value of our spatial predictor selection approach, we implement rigorous comparisons with baselines including:

- **Persistence models** (assuming tomorrow's temperature equals today's)
- **Climatological means** (historical average for each calendar day)

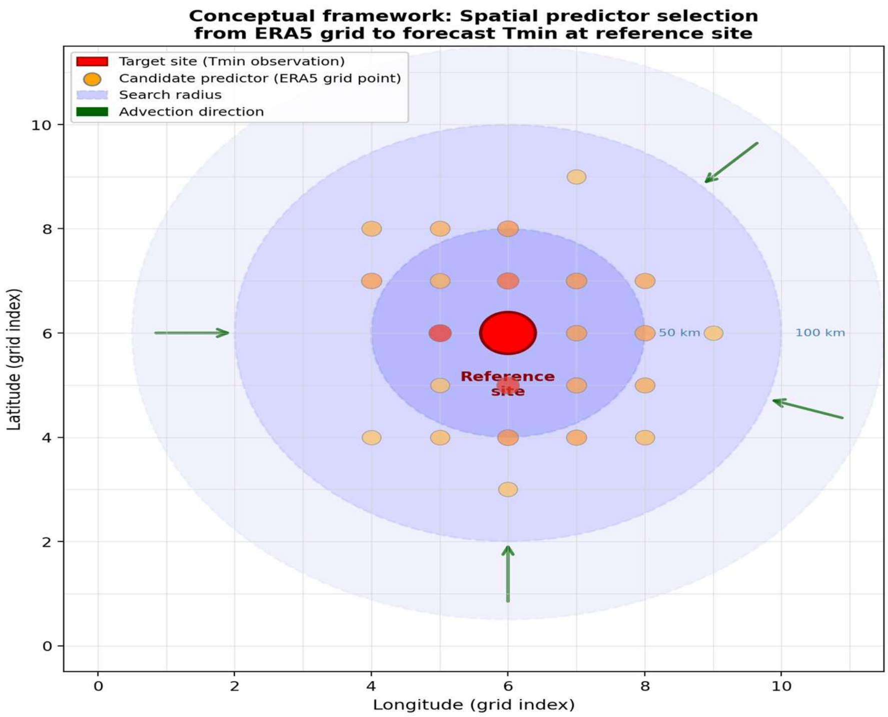

__Figure 1.__ Conceptual framework illustrating the spatial predictor selection approach. The target site (red) is surrounded by candidate ERA5 grid points at varying distances (search radii). Point color intensity indicates

predictor relevance as determined by the selection algorithm. Arrows represent potential advection directions carrying information from distant locations.

1.4 Data limitations and scope of results

A crucial caveat must be stated upfront regarding the interpretation of predictive performance metrics presented in this study. All predictor data come from ERA5 reanalysis (Hersbach et al., 2020), while target observations (minimum temperatures) come from independent NCEI-NOAA station records. ERA5 represents a retrospective analysis that assimilates all available observations and applies sophisticated data assimilation techniques to produce an optimal, physically consistent reconstruction of past meteorological conditions.

Consequently, the MAE values reported in this study are NOT representative of operational forecasting performance that would be obtained using real-time NWP model outputs. ERA5 data benefit from:

- Complete spatial and temporal coverage with no missing data
- Assimilation of all available observations, including those not available in real-time
- Physical consistency optimized through retrospective analysis
- Absence of bias and drift inherent to forecast models

Therefore—and this is the central thesis of our work—while absolute MAE values are not transferable to operational contexts, the methodology for identifying relevant predictors and their spatial configuration remains valid. The physical relationships and spatial structures that emerge from our analysis reflect genuine atmospheric processes. The predictor sets identified through this methodology can be applied using operational forecast data, albeit with expected degradation in absolute performance.

This advantage of reanalysis-based predictors may, however, be partially counterbalanced in operational settings by the use of high-resolution short-range NWP forecasts, which can better capture local-scale processes despite their inherent forecast uncertainty. Additionally, a more judicious selection of features (variables) could also enhance the results.

1.5 Originality and contributions

This work makes several contributions to the field of statistical temperature forecasting:

1. **Systematic spatial exploration:** Unlike approaches that use predefined sets of stations or grid points, our methodology systematically explores geographic space to identify optimal predictor locations
2. **Multi-site comparative analysis:** By applying a consistent methodology to eight climatically diverse sites, we can characterize how optimal predictor configurations vary across local climate regimes
3. **Rigorous baseline validation:** Our comparison with persistence, climatology, and purely local models provides clear evidence of the added value of spatial predictor selection
4. **Physical interpretability:** The identified predictor sets can be interpreted in terms of known meteorological processes (advection, radiative effects, maritime influences)
5. **Open science and reproducibility:** All code, methodological details, and results will be made freely available via repositories such as GitHub and Zenodo, and Docker containers. The repository will be publicly released within 8 to 10 weeks of this preprint
6. **Approach genericity:** Although illustrated on minimum temperature, the methodology is applicable to other meteorological variables and other domains

2. Data

2.1 Study area and reference sites

This study focuses on Western Europe, covering a geographic domain bounded by latitudes 36.45°N to 63.16°N and longitudes 15.19°W to 18.44°E. This region encompasses a wide range of climatic conditions (Peel et al., 2007), from Mediterranean climates in the south to oceanic and semi-continental climates in the north and east, providing an ideal testbed for evaluating the spatial variability of optimal predictor configurations.

Figure 2. *Geographic distribution of the eight reference sites across Western Europe. The background shows the ERA5 grid domain used for predictor extraction.*

Eight reference sites were selected to represent this climatic diversity (Table 1, Figure 2). The sites, located in the United Kingdom and France, include both coastal and inland locations, covering oceanic, semi-continental, and Mediterranean climate types.

Table 1. *Reference sites used in this study.*

Site	**Lat. (°N)**	**Lon. (°E)**	**Country**	**Climate**	**Setting**
Birmingham	52.42	-1.83	UK	Oceanic (Cfb)	Inland
Brest	48.44	-4.41	France	Oceanic (Cfb)	Coastal
Edinburgh	55.97	-3.21	UK	Oceanic (Cfb)	Coastal
Lyon	45.73	5.08	France	Semi-cont. (Cfb)	Inland
Nice	43.65	7.21	France	Medit. (Csa)	Coastal
Paris	48.72	2.38	France	Oceanic (Cfb)	Inland
Plymouth	50.35	-4.12	UK	Oceanic (Cfb)	Coastal
Strasbourg	48.55	7.64	France	Semi-cont. (Cfb)	Inland

2.2 Reference data: observed daily minimum temperatures

The target variable for this study—observed daily minimum temperature (T_{min})—was obtained from the NCEI-NOAA Daily Summaries database. Data were downloaded in CSV format for each of the eight reference sites.

The observation period spans 21 years, from 2004 to 2024 inclusive, providing 7,671 daily observations per site. This extended period captures a wide range of meteorological conditions, including extreme events, and ensures robust statistical analysis.

It is essential to emphasize that these observed temperatures are entirely independent from the ERA5 predictor data described below. This separation between target observations (station-based measurements) and predictor fields (reanalysis products) is fundamental to the validity of our predictor selection methodology.

2.3 Predictor data: ERA5 reanalysis

What is a reanalysis? A reanalysis is a systematic reprocessing of historical meteorological observations using a fixed, modern data assimilation system and numerical weather prediction model (Hersbach et al., 2020). Unlike operational forecasts that evolve over time as models are updated, reanalyses provide temporally consistent datasets by applying the same methodology throughout the entire period. ERA5, produced by the European Centre for Medium-Range Weather Forecasts (ECMWF), is the fifth generation of such reanalyses and currently represents the state of the art in global atmospheric reconstruction.

Grid specifications: ERA5 data are provided on a regular latitude-longitude grid with 0.25° × 0.25° horizontal resolution (approximately 28 km at mid-latitudes). For our study domain [36.45°N–63.16°N, 15.19°W–18.44°E], this corresponds to approximately 107 latitude points × 135 longitude points, yielding roughly 14,000 grid cells.

2.4 Predictor definition

In this study, a predictor is formally defined as a triplet (variable, latitude, longitude) associated with a daily time series. For instance, "mean sea level pressure at grid point (48.25°N, 2.50°E)" constitutes a single predictor.

Formal definition: The total predictor space is defined as the Cartesian product:

$$P = V \times \Lambda \times \Phi$$

where V = {26 meteorological variables}, Λ = {107 latitude values}, and Φ = {135 longitude values}.
Total candidate space: $|P|$ = 362,333 potential predictors. This number is lower than the theoretical maximum (26 × 107 × 135 = 375,570) because certain variable–location combinations are undefined (e.g., sea surface temperature over land, soil temperature over ocean).

2.5 Predictor variables

Daily minimum temperature (T_{min}) results from a complex interplay of physical processes, primarily nocturnal radiative cooling modulated by atmospheric and surface conditions (Oke, 1987). The predictor variables selected for this study were chosen to capture the main drivers of T_{min} variability. They fall into six thematic categories:

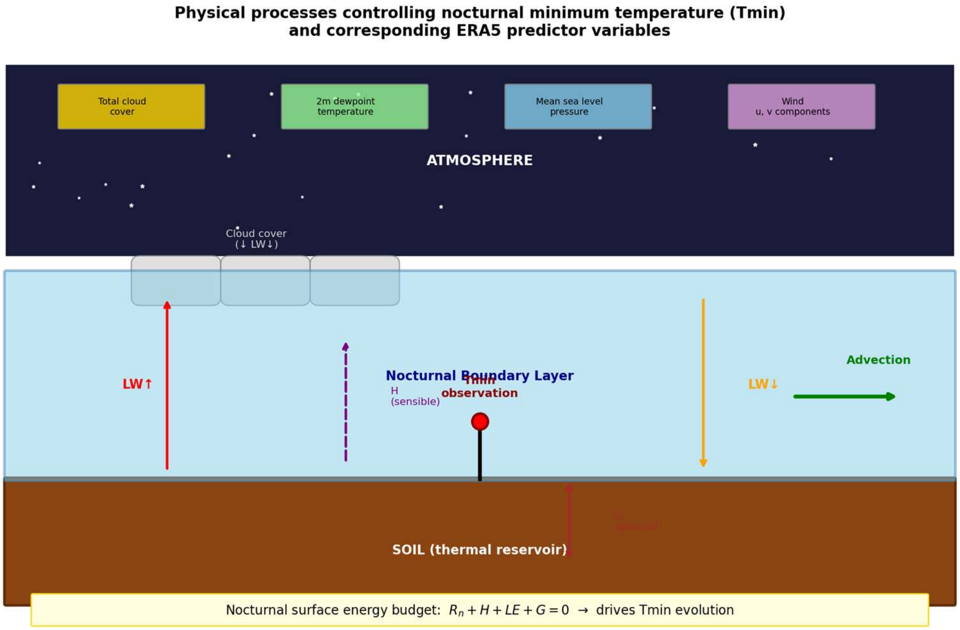

Figure 3. *Schematic representation of physical processes controlling nocturnal minimum temperature (T_{min}). The surface energy budget equation $R_n + H + LE + G = 0$ governs temperature evolution, where R_n is net radiation, H is sensible heat flux, LE is latent heat flux, and G is ground heat flux. ERA5 predictor variables (colored boxes) are linked to these physical processes.*

Radiative balance: Cloud cover (low, medium, high, total), downward thermal and solar radiation, net thermal radiation, and total column water vapour collectively determine the energy exchanges that drive nocturnal cooling (Stull, 1988). Low clouds and atmospheric moisture limit infrared losses, while clear skies promote strong radiative cooling.

Advection and synoptic conditions: Wind components (u, v) and gusts characterize air mass origin and atmospheric mixing. Mean sea level pressure indicates synoptic regime—anticyclonic conditions favour calm, clear nights with low T_{min}, while cyclonic conditions bring clouds and milder nights.

Boundary layer dynamics: Boundary layer height (minimum and maximum) reflects atmospheric stability (Stull, 1988). A shallow nocturnal boundary layer promotes thermal inversions and radiative decoupling, leading to pronounced surface cooling.

Surface and soil state: Skin temperature and soil temperatures at two depths capture surface thermal inertia and heat exchanges with the atmosphere. Soil moisture modifies thermal conductivity and capacity. Snow depth, through its high albedo and insulating properties, strongly influences radiative cooling.

Surface energy fluxes: Latent and sensible heat fluxes, along with evaporation, complete the surface energy budget that governs temperature evolution from day to night.

Thermal persistence: The previous day's T_{min} and dewpoint temperature provide strong baseline predictors through temporal autocorrelation, with dewpoint additionally serving as a theoretical lower bound under saturation conditions.

Table 2. *ERA5 predictor variables used for daily T_{min} forecasting.*

Variable name	Description	Unit
10m_u_component_of_wind_daily_mean	Zonal wind at 10 m (daily mean)	m/s
10m_v_component_of_wind_daily_mean	Meridional wind at 10 m (daily mean)	m/s
10m_wind_gust_since_previous_post_processing_daily_max	Maximum wind gust at 10 m	m/s
2m_temperature_daily_minimum	Minimum air temperature at 2 m	K
2m_dewpoint_temperature_daily_minimum	Minimum dewpoint temperature at 2 m	K

boundary_layer_height_daily_minimum / maximum	Boundary layer height (daily min / max)	m
evaporation_daily_sum	Surface evaporation (daily accumulated)	m
low_cloud_cover_daily_mean	Low cloud cover (daily mean)	0–1
medium_cloud_cover_daily_mean	Medium cloud cover (daily mean)	0–1
high_cloud_cover_daily_mean	High cloud cover (daily mean)	0–1
total_cloud_cover_daily_mean	Total cloud cover (daily mean)	0–1
mean_sea_level_pressure_daily_mean	Mean sea level pressure (daily mean)	Pa
sea_surface_temperature_daily_mean	Sea surface temperature (daily mean)	K
skin_temperature_daily_minimum	Minimum surface skin temperature	K
soil_temperature_level_1_daily_minimum	Minimum soil temperature (layer 1)	K
soil_temperature_level_2_daily_minimum	Minimum soil temperature (layer 2)	K
surface_latent_heat_flux_daily_sum	Latent heat flux (daily accumulated)	J/m²
surface_sensible_heat_flux_daily_sum	Sensible heat flux (daily accumulated)	J/m²
surface_net_thermal_radiation_daily_sum	Net thermal radiation at surface (daily sum)	J/m²
surface_solar_radiation_downwards_daily_sum	Downward solar radiation at surface (daily sum)	J/m²
surface_thermal_radiation_downwards_daily_mean	Downward thermal radiation at surface (daily mean)	W/m²
total_column_water_vapour_daily_mean	Total column water vapour (daily mean)	kg/m²
total_precipitation_daily_sum	Total precipitation (daily accumulated)	m
volumetric_soil_water_layer_1_daily_mean	Volumetric soil water content (layer 1)	m³/m³
snow_depth_daily_mean	Snow depth (daily mean)	m

2.6 Potential redundancies

Several groups of variables exhibit expected collinearity. Cloud cover variables (total, low, medium, high) are mechanically related, as are the various temperature fields (2 m air, skin, soil layers). Radiative fluxes are partly determined by cloudiness and moisture content. These redundancies are not necessarily detrimental: gradient boosting methods (e.g., XGBoost) and neural networks typically handle correlated features without significant performance degradation (Chen and Guestrin, 2016). However, for model interpretation—particularly when computing feature importance or SHAP values—collinearity may dilute importance across redundant variables.

2.7 Data processing and storage

The predictor data (NetCDF format from ERA5) and reference observations (CSV format from NCEI-NOAA) were integrated into a unified SQLite database to facilitate data management and querying. This standardization offers several advantages:

- Uniform access to heterogeneous source formats through a single interface
- Efficient querying via SQL for data exploration and extraction
- Reproducibility through explicit data transformations
- Portability of the complete dataset as a single file

2.8 Objective and evaluation framework

A fundamental clarification is required regarding the role of performance metrics in this study. The objective is *not* to minimize the mean absolute error (MAE) in absolute terms. Rather, the objective is to **identify optimal sets of spatially distributed predictors**—that is, to determine which variables at which geographic locations provide the most informative signal for T_{min} forecasting.

Evaluation metric: The Mean Absolute Error (MAE) serves as a comparative criterion:

$$MAE_{config} = (1/N)\ \Sigma_i\ |y_i - \hat{y}_i|$$

Configuration ranking: $config_A \succ config_B \Leftrightarrow MAE_A < MAE_B$

In this context, the MAE serves as a **compass** rather than a destination. It provides a quantitative criterion for comparing and ranking predictor configurations, guiding the search toward more informative predictor sets. The absolute MAE value is less important than its *relative ranking* across configurations. A configuration yielding MAE = 1.5°C is preferred over one yielding MAE = 1.8°C, regardless of whether these values would be considered "good" or "poor" in an operational context.

This perspective has important implications for result interpretation. We prioritize the stability and interpretability of selected predictor sets over marginal performance improvements. A predictor configuration that consistently emerges across different model types and validation periods is more valuable than one that achieves slightly lower MAE but lacks robustness.

3. Methodology

This section describes the predictor selection methodology, including the definition of the search space, the selection algorithm, the optimization of the number of predictors, and the model configuration used for evaluation. The overall objective is not to achieve the best possible forecast accuracy per se, but rather to identify the most informative predictors for minimum temperature prediction. In this framework, the Mean Absolute Error (MAE) serves as a guiding criterion—a compass directing the search toward predictors that carry the strongest predictive signal (cf. Lakshmanan et al., 2015).

3.1 Temporal Window Analysis

Rationale

A critical methodological question in predictor selection for minimum temperature forecasting concerns the temporal depth of atmospheric information required (Box and Jenkins, 1976). While the atmospheric state on the current day provides direct predictive information for the minimum temperature on the following day, the inclusion of lagged variables from the previous two days could potentially capture synoptic-scale memory effects, particularly for continental stations where advective processes may exhibit multi-day persistence (Holmberg et al., 2024).

This experiment aimed to determine whether extending the temporal window beyond a single day improves predictive performance, or whether the atmospheric state at current day already encodes sufficient information, rendering lagged predictors redundant. The relevance of lagged predictors can be quantified through the temporal autocorrelation function. For a time series X, the autocorrelation at lag k is defined as:

$$\rho(k) = Cov(X_p, X_{p-k}) / Var(X)$$

where ρ(k) represents the correlation between observations separated by k time steps. High autocorrelation at lags k = 1 or k = 2 would suggest that including predictors from days D-1 or D-2 might improve forecast skill.

Experimental Design

Following the approach of lag selection in autoregressive modeling (Hyndman and Athanasopoulos, 2021), three temporal window configurations were evaluated: (1) a single-day window (current day only); (2) a two-day window (incorporating a one-day lag); and (3) a three-day window (incorporating up to two-day lags). Each configuration was tested across four climatically contrasting stations: Birmingham (UK, oceanic), Brest (France, maritime), Nice (France, Mediterranean), and Strasbourg (France, continental).

For each station-window combination, the predictor selection algorithm was executed with five different random seeds to assess stability. Three machine learning models were applied: linear regression (as baseline), LightGBM, and XGBoost. Performance was measured using mean absolute error (MAE) on the test dataset (2023-2024), with results reported as mean ± standard deviation across seeds.

Results were stored in JSON format with the following structure: for each window size (win_size_1, win_size_2, win_size_3), nested objects contain station-level results with model-specific MAE averages and standard deviations, plus mean elapsed computation time.

Results

Table 3 presents the MAE results for XGBoost, which consistently outperformed the other models across all configurations.

Table 3. Mean absolute error (°C) by station and temporal window size (XGBoost model). Bold values indicate best performance. W1 = 1-day window, W2 = 2-day window.

Station	Window 1	Window 2	Window 3	Best
Birmingham	**0.930 ± 0.009**	0.952 ± 0.016	0.946 ± 0.010	W1
Brest	**1.352 ± 0.041**	1.372 ± 0.037	1.375 ± 0.030	W1
Nice	**0.829 ± 0.019**	0.837 ± 0.008	0.838 ± 0.011	W1
Strasbourg	1.312 ± 0.024	**1.295 ± 0.014**	1.325 ± 0.020	W2
Avg. time	*~40 min*	*~48 min*	*~55 min*	

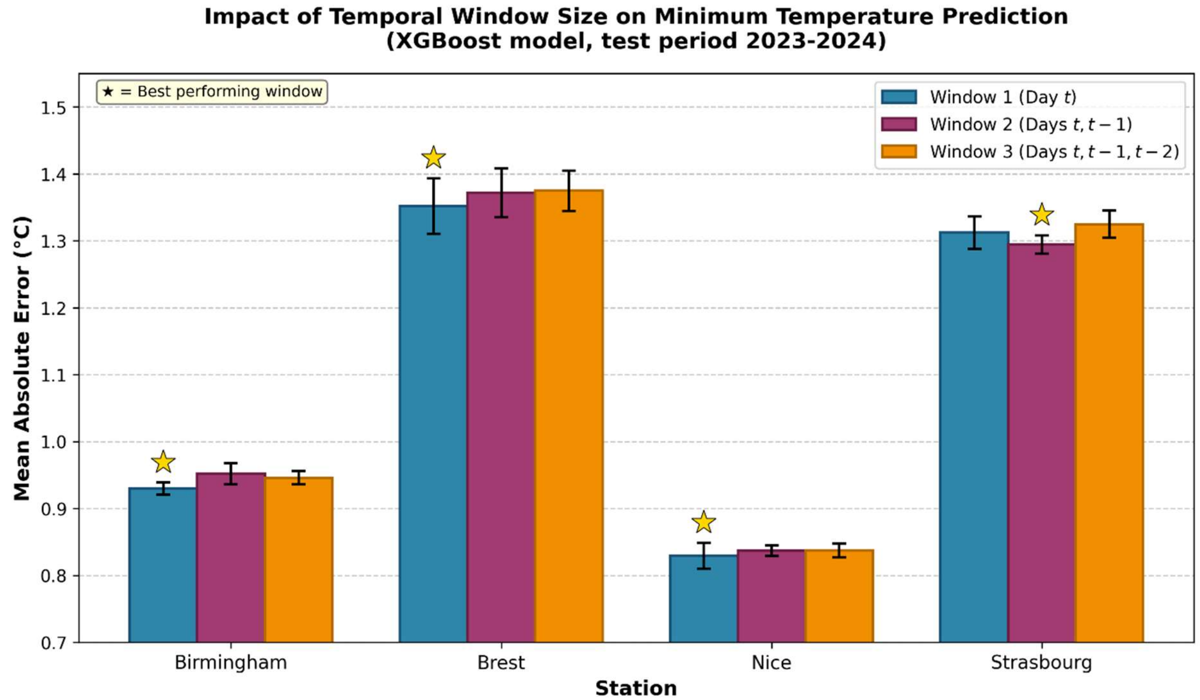

Figure 4. *Comparison of MAE across temporal window sizes for each station. Error bars represent ± one standard deviation across five random seeds.*

Analysis

The single-day temporal window achieved optimal or near-optimal performance for three of the four stations, consistent with the principle of parsimony in time series modeling (Burnham and Anderson, 2002). Birmingham exhibited the clearest advantage for window 1, with a MAE reduction of 2.3% compared to window 2. Similar patterns emerged for Brest (−1.5%) and Nice (−1.0%). These results suggest that for oceanic, maritime, and Mediterranean climates, the atmospheric state on the current day contains sufficient predictive information for minimum temperature forecasting for the following day.

Strasbourg presented the sole exception, with the two-day window outperforming the single-day configuration by 1.3%. This finding aligns with the continental character of the station, where synoptic-scale processes—particularly cold air advections from northeastern Europe—may exhibit greater temporal persistence. The extended window likely captures the progressive establishment of high-pressure systems and associated radiative cooling conditions that influence minimum temperatures over multiple days.

The three-day window consistently underperformed relative to shorter configurations, indicating that atmospheric information beyond the previous day introduces noise rather than useful signal. Standard deviations remained comparable across window sizes (typically 1-3% of MAE), suggesting that the stochastic variability inherent to the selection algorithm does not confound these comparisons.

Computation time increased approximately linearly with window size, with the three-day window requiring 35% more time than the single-day configuration. This overhead, combined with degraded predictive performance, reinforces the practical advantage of the parsimonious approach.

Conclusion

The single-day temporal window was adopted as the default configuration for subsequent analyses. This choice reflects both empirical performance—optimal for 75% of stations tested—and the principle of parsimony advocated by Box and Jenkins (1976) for time series modeling. The atmospheric state at current day appears to encode the relevant synoptic and mesoscale information required for minimum temperature prediction, with lagged variables providing marginal or negative value.

This finding carries important implications for the physical interpretability of selected predictors: features identified under the single-day paradigm represent contemporaneous atmospheric drivers rather than lagged proxies, simplifying their meteorological interpretation and enhancing their potential transferability to operational forecasting contexts using numerical weather prediction outputs.

3.2 Predictor Search Space

The predictor selection algorithm explored a search space defined by the combination of ERA5 variables (described in Section 2) and spatial locations within a fixed radius around each target station. ERA5 reanalysis (Hersbach et al., 2020) was deliberately employed to approximate an optimal atmospheric state, allowing the intrinsic predictive value of each variable to be assessed independently of operational forecast errors.

Spatial domain

For each station, the candidate predictor pool comprised all ERA5 grid points within a radius R = 540 km. At the native ERA5 resolution of 0.25°, this radius encompasses a variable number of grid points depending on station latitude. Because ERA5 uses a regular latitude-longitude grid, the physical spacing between grid points in the zonal direction decreases with increasing latitude ($\Delta x \approx 28$ km × cos(ϕ), where ϕ is latitude). Consequently, higher-latitude stations capture more grid points within the same 540 km radius.

Across the eight stations, the total number of candidate predictors (grid points × variables) ranged from approximately 41,000 (Nice, 43.7°N) to 53,000 (Edinburgh, 55.9°N), with a median of approximately 45,000. This latitudinal dependence reflects the convergence of meridians rather than any methodological inconsistency: the haversine distance metric ensures that all stations sample the same physical area ($\pi \times 540^2 \approx 916{,}000$ km^2), but the grid point density within that area varies with latitude.

The 540 km radius was chosen to capture synoptic-scale atmospheric patterns that influence local minimum temperatures (Holton and Hakim, 2013), while remaining computationally tractable.

Temporal configuration

Predictors were extracted from ERA5 fields for the current day to forecast the overnight minimum temperature (i.e., the T_{min} for the following day). This configuration reflects an operational forecasting scenario where atmospheric conditions observed during the day are used to predict the following night's minimum temperature.

In addition to the 26 ERA5 variables, the observed minimum temperature at the target station (from the NOAA GSOD dataset; Menne et al., 2012) **was included as a candidate predictor**. This allows the algorithm to exploit persistence—the tendency for consecutive days to have similar temperatures—where climatologically appropriate.

3.3 Predictor Selection Algorithm

Given the high dimensionality of the search space (ranging from ~41,000 to ~53,000 candidates depending on station latitude), exhaustive evaluation of all possible predictor combinations is computationally infeasible. The number of possible subsets of size k from n candidates is given by the binomial coefficient:

$$C(n, k) = n! / [k! \times (n - k)!]$$

Even for the smallest candidate pool (n ≈ 41,000 at Nice) and a modest subset size (k = 90), this yields an astronomically large number of combinations (~10^{200}), rendering exhaustive search impossible. The latitude-induced variation in candidate pool size across stations (up to ~30% difference between Nice and Edinburgh) does not materially affect this conclusion, as all stations face comparably intractable combinatorial spaces. Instead, an iterative optimization algorithm was employed to identify near-optimal predictor subsets.

Objective function

The algorithm sought to minimize the Mean Absolute Error (MAE) on a held-out validation dataset. The MAE is defined as:

$$MAE = (1/n) \times \Sigma_i |y_i - \hat{y}_i|$$

where y_i is the observed minimum temperature, $\hat{y}_i$ is the predicted value, and n is the number of observations. MAE was preferred over Mean Squared Error (MSE) as it is less sensitive to outliers and provides a directly interpretable measure in °C (Willmott and Matsuura, 2005).

For each candidate predictor subset, a **linear regression** model was trained on the learning dataset and evaluated on the validation dataset. The MAE on the validation set served as the criterion guiding the search. Linear regression was chosen for its computational efficiency, enabling rapid evaluation of thousands of candidate subsets during the iterative search process.

At the end of the search process, the final predictor set was evaluated using gradient boosting models (LightGBM and XGBoost), which achieved lower MAE than linear regression due to their ability to capture non-linear relationships. The systematic use of gradient boosting during the search would have substantially increased computational time, hence the two-stage approach: linear regression for search guidance, gradient boosting for final evaluation.

Search strategy

The feature search algorithm iteratively explored the predictor space, evaluating candidate subsets and progressively refining the predictor set toward lower validation MAE. The search was guided by heuristics that balance exploration of new predictor combinations with exploitation of promising solutions identified in previous iterations. This approach belongs to the family of metaheuristic optimization methods, which have proven effective for high-dimensional subset optimization problems (Xue et al., 2016).

Stopping criterion

The algorithm employed an early stopping criterion based on lack of improvement. If no new best solution (lower validation MAE) was found within P = 60 consecutive iterations, the search terminated and returned the predictor subset corresponding to the lowest validation MAE encountered during the entire run. This patience-based stopping criterion (Prechelt, 1998) balances thorough exploration against computational cost.

Stochastic variability

Due to the stochastic nature of the search algorithm, different runs with different random seeds generally converge to different predictor subsets. To assess the robustness of the results, five independent runs were performed for each station, each initialized with a different random seed. This allows analysis of both the consistency of predictor selections across runs and the variability in prediction performance.

3.4 Predictor Count Optimization

3.4.1 Rationale

The number of predictors retained by the search algorithm represents a critical trade-off between model expressiveness and parsimony. Too few predictors may fail to capture the full complexity of atmospheric drivers influencing minimum temperatures, while excessive predictors risk introducing redundant information, increasing computational cost, and potentially degrading generalization through overfitting.

3.4.2 Experimental Design

Four predictor counts were evaluated: 50, 70, 90, and 110. Based on the results of Section 3.1, all experiments used a single-day temporal window (current day only). Tests were conducted across the same four climatically contrasting stations: Birmingham, Brest, Nice, and Strasbourg. For each configuration, the predictor selection algorithm was executed with five different random seeds, and performance was evaluated using XGBoost on the test dataset (2023–2024). Mean computation time was recorded to assess the computational cost of each configuration.

3.4.3 Results

Table 4 presents the MAE results for each station and predictor count, along with the relative improvement between successive configurations.

Station	50	70	90	110	Best
Birmingham	0.943	0.930	0.920	**0.901**	110
Brest	1.367	1.352	1.340	**1.331**	110
Nice	0.850	0.829	**0.810**	0.813	90
Strasbourg	1.315	1.312	1.294	**1.290**	110
Avg. time	*~23 min*	*~40 min*	*~60 min*	*~78 min*	

Table 4. Mean absolute error (°C) by station and number of predictors (XGBoost model). Bold values indicate best performance for each station.

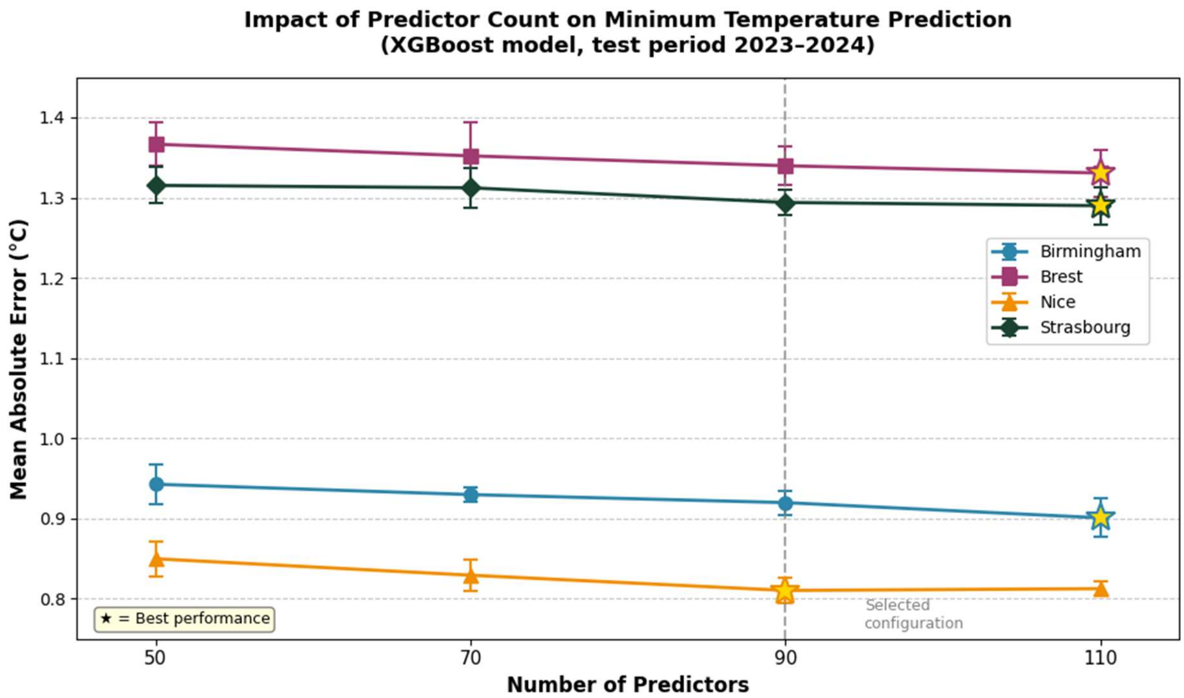

Figure 5. *Sensitivity of prediction accuracy to predictor subset size (XGBoost model, test period 2023–2024). The vertical dashed line indicates the selected configuration (90 predictors); stars denote best performance per station.*

3.4.4 Analysis

The results reveal a consistent pattern of diminishing returns as predictor count increases. All stations exhibited substantial improvement when moving from 50 to 70 predictors, with relative MAE reductions ranging from 0.2% (Strasbourg) to 2.5% (Nice). The transition from 70 to 90 predictors yielded further gains across all stations, ranging from 0.9% (Brest) to 2.3% (Nice).

Beyond 90 predictors, the behavior diverged across stations. Birmingham continued to benefit from additional predictors, with a 2.1% improvement at 110 predictors—the largest marginal gain observed in the 90-to-110 transition. This suggests that the oceanic climate of central England, influenced by multiple synoptic-scale drivers, requires a larger predictor set to capture its full complexity. Brest and Strasbourg showed marginal improvements (0.7% and 0.3%, respectively), while Nice exhibited a slight performance degradation (+0.3%), indicating potential overfitting when the predictor count exceeds the intrinsic dimensionality of the prediction problem.

The relationship between predictor count and computational cost proved approximately linear, with execution time increasing from ~23 minutes at 50 predictors to ~78 minutes at 110 predictors. This represents a 3.4-fold increase in computation time for a modest improvement in predictive performance.

Standard deviations remained stable across configurations (typically 1.5–2.5% of MAE), indicating that the search algorithm achieved consistent convergence regardless of the predictor count constraint.

3.4.5 Conclusion

Based on these results, 90 predictors was selected as the default configuration for subsequent analyses. This value represents the point of diminishing returns for three of the four stations tested: beyond this threshold, performance gains become marginal (Brest, Strasbourg) or negative (Nice), suggesting that additional predictors introduce redundancy or noise rather than useful information.

The choice of 90 predictors also offers a practical compromise between predictive accuracy and computational cost. Compared to the 110-predictor configuration, it reduces execution time by approximately 20% while sacrificing less than 1% in MAE for most stations.

Although Birmingham exhibited continued improvement at 110 predictors, a uniform configuration was retained for methodological consistency. This facilitates cross-station comparison of selected predictors and avoids introducing station-specific tuning that could complicate interpretation. The modest performance difference (0.019°C) was deemed insufficient to justify a heterogeneous approach.

3.5 Model Configuration

Data partitioning

The available data (2004–2024) was partitioned chronologically into three non-overlapping periods, following best practices for time series forecasting (Bergmeir and Benítez, 2012):

Learning set (85%): January 2004 to approximately early 2020. Used for training the regression models during predictor selection.

Validation set (15%): Approximately 2020 to December 2022. Used to evaluate candidate predictor subsets and guide the selection algorithm. The MAE on this set served as the optimization objective.

Test set: January 2023 to December 2024. Held out entirely during predictor selection and used only for final performance evaluation. This strict temporal separation ensures that reported test results reflect true out-of-sample performance.

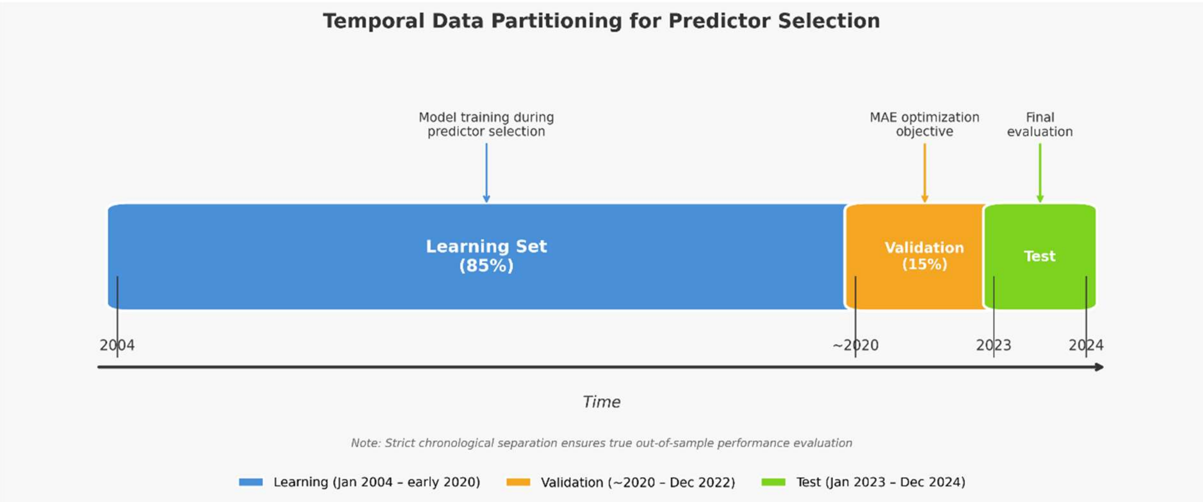

Figure 6*. Schematic diagram of temporal data partitioning. The chronological split ensures strict separation between training, validation, and test periods.*

Regression models

Three regression models were evaluated for each selected predictor subset:

Linear regression: Ordinary least squares (OLS) regression, minimizing the sum of squared residuals. This model provides a simple baseline and interpretable coefficients, and was used during the predictor search phase due to its computational efficiency.

LightGBM: A gradient boosting framework using histogram-based learning, optimized for efficiency and scalability (Ke et al., 2017).

XGBoost: An optimized gradient boosting implementation with L1 and L2 regularization to prevent overfitting (Chen and Guestrin, 2016).

XGBoost consistently achieved the lowest mean MAE across all eight stations, and was therefore adopted as the primary model for reporting results. The following hyperparameters were used: learning rate $\eta = 0.02$, maximum tree depth $d = 6$, column subsampling ratio = 0.8, row subsampling ratio = 0.8, L1 regularization $\alpha = 0.1$, L2 regularization $\lambda = 0.1$. These values were selected based on common recommendations in the literature (Chen and Guestrin, 2016) rather than extensive tuning, as the focus of this study is predictor identification rather than model optimization.

Predictor importance metrics

To analyze which predictors contribute most to model performance, XGBoost's built-in feature importance metrics were extracted. The *gain* metric was used as the primary importance measure. For a given predictor j, the gain G_j is defined as the sum of loss reductions achieved by all splits using that predictor:

$$G_j = \Sigma_t\, \Sigma_s {\in} S_{jt}\, \Delta L(s)$$

where the outer sum is over all trees t in the ensemble, S_{jt} is the set of splits using predictor j in tree t, and $\Delta L(s)$ is the reduction in the loss function achieved by split s. This metric captures both the frequency with which a predictor is selected for splitting and the magnitude of improvement each split provides.

Computational settings

The model was developed and tested on a standard virtual environment with 8 vCPUs (AMD EPYC 9645) and 16 GB of RAM. This setup is intentionally equivalent to a standard consumer-grade desktop computer (e.g., an AMD Ryzen 7 system). Our goal was to ensure that the proposed forecasting method remains computationally accessible and can be implemented on affordable, everyday hardware without requiring expensive server clusters or specialized GPUs.

3.6 Evaluation Metrics

Model performance was assessed using multiple complementary metrics computed on the independent test set (2023–2024):

Mean Absolute Error (MAE): Primary performance metric, as mathematically defined above, representing the average magnitude of prediction errors in °C.

Coefficient of determination (R^2): Proportion of variance in observed Tmin explained by the model, defined as:

$$R^2 = 1 - [\Sigma_i(y_i - \hat{y}_i)^2 / \Sigma_i(y_i - \bar{y})^2]$$

where $\bar{y}$ is the mean of observed values.

Bias: Mean signed error, indicating systematic over- or under-prediction:

$$Bias = (1/n) \times \Sigma_i\, (\hat{y}_i - y_i)$$

Success rates: Percentage of predictions within ±1°C and ±2°C of observations, providing operationally relevant accuracy measures.

Error percentiles (P50, P90, P95): Distribution of absolute errors, characterizing typical and worst-case performance.

Seasonal and annual breakdowns: MAE computed separately for each season (DJF, MAM, JJA, SON) and each year (2023, 2024) to identify temporal patterns in prediction difficulty.

Additionally, two baseline methods were computed for comparison: *persistence* (using the previous day's observed Tmin as the forecast) and *climatology* (using the historical mean Tmin for each calendar date). These baselines provide context for interpreting model skill (Jolliffe and Stephenson, 2012).

4. Results

4.1 Overall Performance

The predictor selection algorithm was applied to eight meteorological stations spanning diverse European climates. Table 5 summarizes the prediction performance on the independent test period (2023-2024) using the XGBoost regression model (Chen and Guestrin, 2016) driven by 90 selected predictors.

Table 5. *Prediction performance for minimum temperature (Tmin) at eight European stations. MAE: Mean Absolute Error; values are averages across five independent runs with different random seeds.*

Station	Climate	MAE (°C)	R^2	Bias (°C)	≤1°C (%)	≤2°C (%)	P95 (°C)
Nice	Mediterranean	0.81	0.972	-0.13	68.9	93.3	2.15
Birmingham	Oceanic	0.92	0.936	-0.01	62.2	91.4	2.30
Plymouth	Oceanic	1.07	0.906	+0.00	54.3	86.0	2.62
Paris	Semi-continental	1.21	0.923	-0.35	50.1	82.1	3.00
Lyon	Semi-continental	1.22	0.946	-0.22	50.2	82.1	3.06
Edinburgh	Oceanic	1.24	0.892	-0.02	50.0	79.1	3.11
Strasbourg	Continental	1.29	0.931	-0.04	48.1	78.5	3.29
Brest	Oceanic	1.34	0.845	+0.11	45.7	77.1	3.31

Prediction accuracy varied substantially across stations, with MAE ranging from 0.81°C (Nice) to 1.34°C (Brest). Mediterranean climate (Nice) proved easiest to predict, with nearly 70% of forecasts within 1°C of observations and over 93% within 2°C. Continental and oceanic climates presented greater challenges, with success rates (≤2°C) between 77% and 91%, consistent with the greater synoptic variability typically affecting these regimes (Wallace and Hobbs, 2006).

The 95th percentile of absolute errors (P95) provides insight into worst-case performance. Even for the most challenging stations (Strasbourg, Brest), P95 remained below 3.5°C, indicating that large errors were relatively rare.

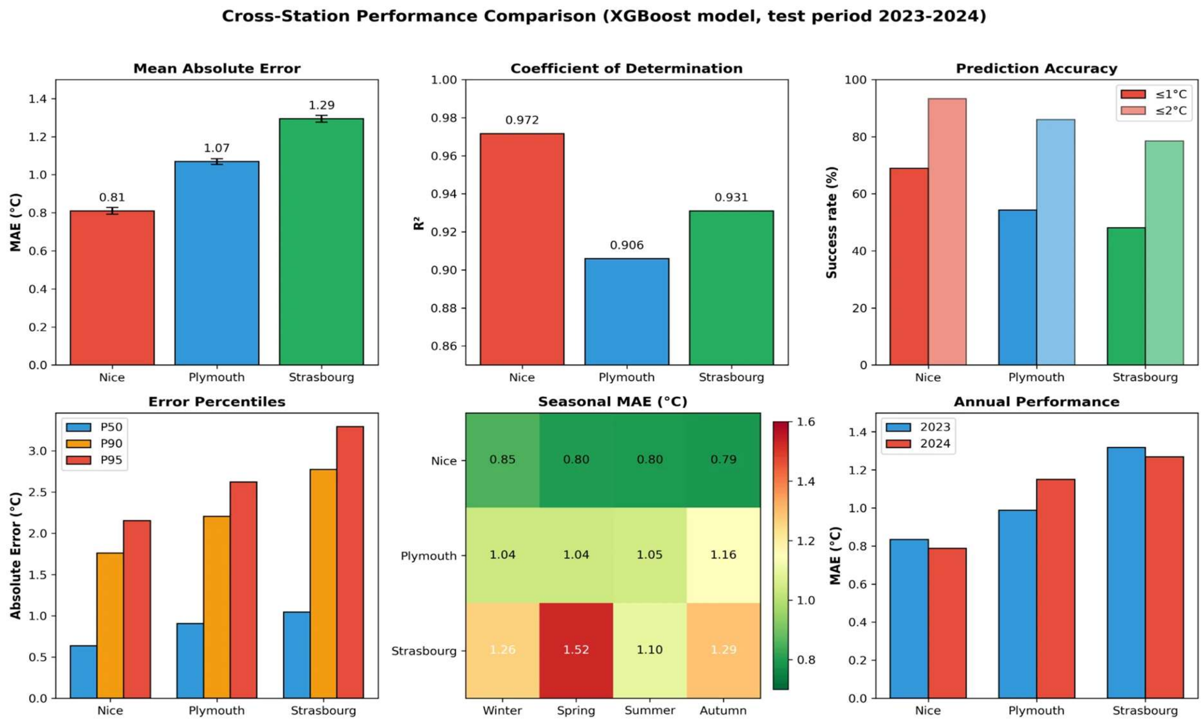

Figure 7. *Cross-station performance comparison for minimum temperature prediction (XGBoost model, test period 2023-2024). Panels show mean absolute error, coefficient of determination, prediction accuracy, error percentiles, seasonal MAE, and annual performance.*

Comparison with baseline methods

To contextualize model performance, Table 6 compares results against two simple baselines: day-ahead persistence (using yesterday's Tmin as tomorrow's forecast) and climatology (historical mean Tmin for the calendar date). Persistence is a well-known strong baseline for short-range temperature forecasting (Wilks, 2011). A parsimonious SARIMAX model with annual Fourier terms (Box et al., 2015) performs similarly to climatology and is clearly outperformed by persistence, confirming the limited relevance of univariate linear models for daily minimum temperature prediction.

Table 6. *Comparison of model performance against baseline methods. Improvement percentages indicate MAE reduction relative to each baseline.*

Station	Model	Persistence	Climatology	vs Pers.	vs Clim.
Nice	0.81	1.25	1.93	-35%	-58%
Birmingham	0.92	1.99	2.56	-54%	-64%
Plymouth	1.07	2.00	2.46	-46%	-56%
Paris	1.21	2.24	2.97	-46%	-59%
Lyon	1.22	2.25	2.98	-46%	-59%
Edinburgh	1.24	2.29	2.59	-46%	-52%
Strasbourg	1.29	2.42	3.09	-47%	-58%
Brest	1.34	2.40	2.73	-44%	-51%

The model reduced MAE by 35-54% compared to persistence and by 51-64% compared to climatology. Notably, the improvement over persistence was smallest at Nice (35%), where the Mediterranean climate naturally exhibits high day-to-day thermal stability. This finding is consistent with the predictor analysis presented in Section 4.3, which reveals a strong persistence signal in the selected predictors for this station.

Seasonal variations

Prediction difficulty varied seasonally, with distinct patterns emerging for different climate types (Table 7).

Table 7. *Seasonal MAE (°C) for each station. Bold values indicate the most challenging season.*

Station	Winter	Spring	Summer	Autumn	Most difficult
Nice	**0.85**	0.80	0.80	0.79	Winter
Birmingham	0.88	1.00	0.78	**1.02**	Autumn
Plymouth	1.04	1.04	1.05	**1.16**	Autumn
Paris	**1.33**	1.19	1.15	1.17	Winter
Lyon	**1.42**	1.19	1.10	1.18	Winter
Edinburgh	1.11	1.28	1.17	**1.40**	Autumn
Strasbourg	1.26	**1.52**	1.10	1.29	Spring
Brest	1.42	1.27	1.22	**1.46**	Autumn

Three distinct seasonal patterns emerged: (1) Oceanic stations (Birmingham, Plymouth, Edinburgh, Brest) showed highest errors in autumn, likely due to increased synoptic variability during the transition from summer to winter regimes (Wallace and Hobbs, 2006); (2) Semi-continental stations (Paris, Lyon) performed worst in winter, when stable boundary-layer conditions and temperature inversions frequently occur (Stull, 1988); (3) Strasbourg (continental) uniquely exhibited peak errors in spring, when transitional weather between winter and summer patterns increases forecast uncertainty.

4.2 Predictor Analysis Methodology

To investigate which atmospheric variables and spatial patterns drive minimum temperature predictions, detailed predictor analyses were conducted for three representative stations: Nice (Mediterranean, best performance), Plymouth (oceanic, intermediate), and Strasbourg (continental, most challenging). These stations were selected to maximize climatic diversity while spanning the full range of observed prediction accuracy.

Variable-level versus grid-point stability

A key methodological finding emerged from comparing predictor selections across five independent runs with different random seeds. While individual grid-point selections showed high variability (with no predictors appearing in all five runs for each station, except for the reference series itself), *variable-level* selections were remarkably stable: 23-24 of 26 ERA5 variables were consistently selected across all runs.

This apparent paradox reflects the high spatial autocorrelation of meteorological fields, whereby nearby grid points convey highly redundant information (von Storch and Zwiers, 1999). The algorithm identifies *which variables matter* robustly, even though the *exact spatial locations* vary between runs. Consequently, the following analyses focus on variable-level importance, aggregating contributions across all grid points of each variable.

Importance metrics

Predictor importance was quantified using XGBoost gain, which measures the total reduction in the loss function attributable to each predictor across all tree splits (Chen and Guestrin, 2016). This metric captures both the frequency with which a predictor is used and the magnitude of its contribution to model accuracy.

4.3 Detailed Analysis: Nice (Mediterranean Climate)

Nice, located on the French Riviera, exhibits a Mediterranean climate characterized by mild winters, warm summers, and thermal stability moderated by the sea. The station achieved the best prediction performance (MAE = 0.81 ± 0.02°C, R^2 = 0.97).

Variable importance

Figure 8 shows the relative importance of ERA5 variables for Nice. The predictor hierarchy revealed several distinctive features:

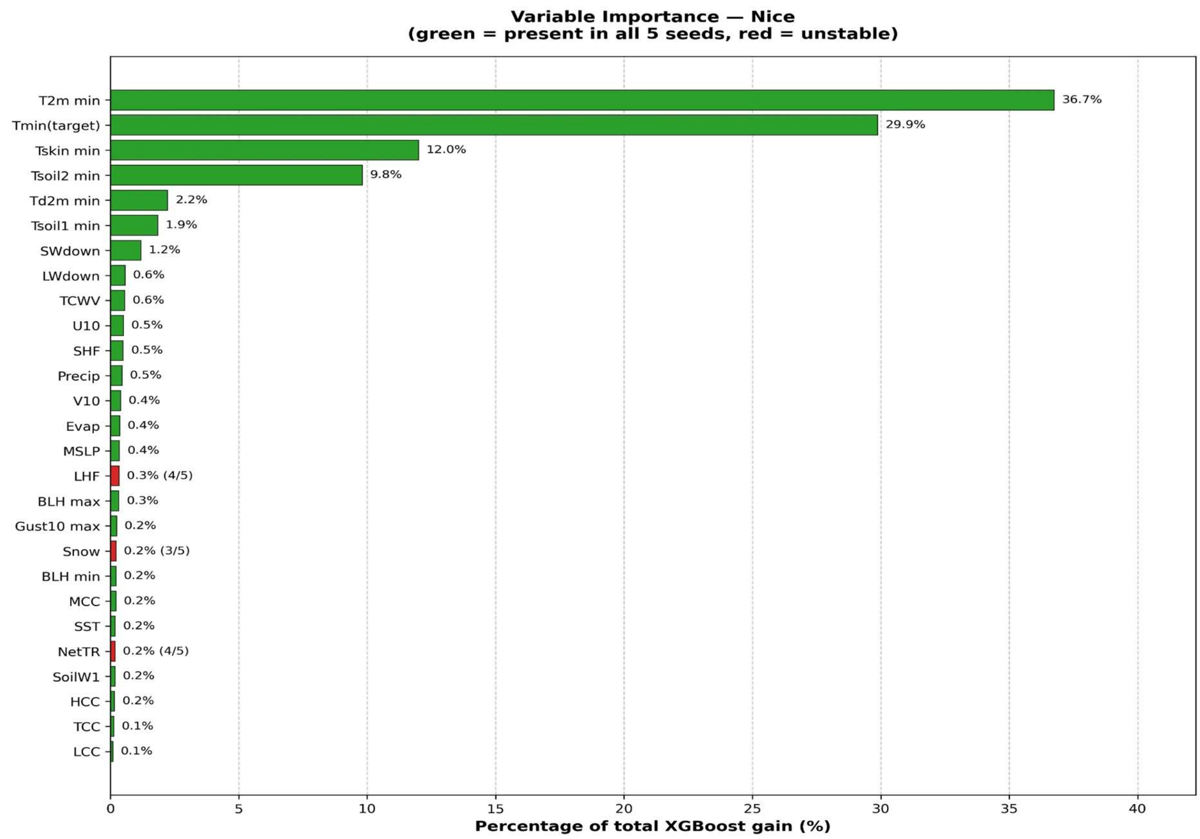

Figure 8. *Variable importance for Nice (Mediterranean climate). Green bars indicate predictors present in all 5 independent runs; red bars indicate unstable selections. The strong persistence signal (Tmin target: 30%) is distinctive of this station.*

(1) *2-meter air temperature minimum (T2m_min)* dominated with 37% of total gain, though this contribution was lower than at other stations (65-66% for Plymouth and Strasbourg). The dominant role of near-surface temperature is consistent with the strong control exerted by local boundary-layer processes under stable nocturnal conditions (Stull, 1988).

(2) *The target variable itself (Tmin reference)* contributed 30% of gain—a strong persistence signal unique to Nice among the three analyzed stations. This reflects the thermal stability of Mediterranean climate, where day-to-day temperature variations are buffered by maritime influence. Such persistence effects are well documented in regions subject to strong oceanic thermal inertia (Wilks, 2011; Oke, 1987).

(3) *Surface temperatures (skin temperature 12%, soil temperature layer 2: 10%)* were more important than at other stations, capturing the land-sea thermal contrast that governs nocturnal cooling in coastal Mediterranean environments (Oke, 1987).

Spatial distribution

Nice exhibited the most spatially dispersed predictor pattern among the three stations, with only 65% of total gain originating within 200 km of the station (compared to 78% for Plymouth and Strasbourg). Selected predictors extended across the northwestern Mediterranean basin, including locations in Italy, southern France, and over the sea. This pattern suggests that the Mediterranean basin functions as a coherent climatic unit for minimum temperature prediction, reflecting the spatial coherence of synoptic-scale meteorological fields (von Storch and Zwiers, 1999).

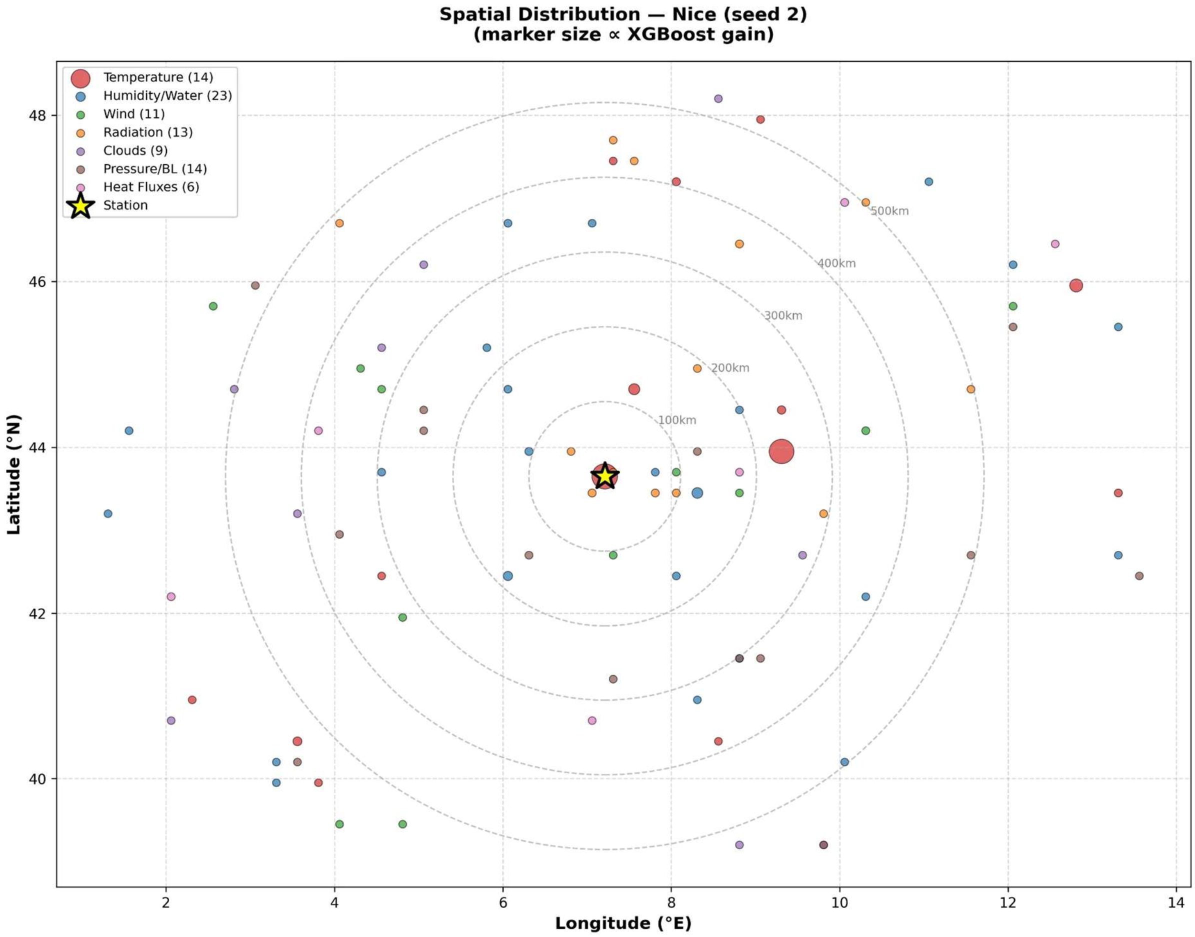

Figure 9. *Spatial distribution of selected predictors for Nice. Marker size is proportional to XGBoost gain. Predictors are dispersed across the northwestern Mediterranean basin, with only 65% of total gain within 200 km.*

4.4 Detailed Analysis: Plymouth (Oceanic Climate)

Plymouth, on the southwest coast of England, experiences a temperate oceanic climate characterized by mild temperatures year-round, high humidity, and frequent weather changes associated with Atlantic frontal systems. Prediction performance was intermediate (MAE = 1.07 ± 0.01°C, R^2 = 0.91).

Variable importance

The predictor hierarchy for Plymouth differed markedly from Nice:

(1) *T2m_min strongly dominated* with 66% of total gain, the highest concentration among the three stations.

(2) *Dewpoint temperature (Td2m)* contributed 16%—a distinctive signature of oceanic climate. The dewpoint captures humidity content of Atlantic air masses, which strongly influences nocturnal cooling rates through its effect on longwave radiation (Brutsaert, 1982).

(3) *Total column water vapour (TCWV: 3%) and meridional wind component (V10: 2%)* provided secondary contributions, reflecting the importance of moisture advection from the Atlantic.

(4) *The persistence signal was negligible* (Tmin reference < 1%), consistent with the changeable nature of oceanic weather where day-to-day conditions vary substantially under the influence of passing frontal systems (Wilks, 2011).

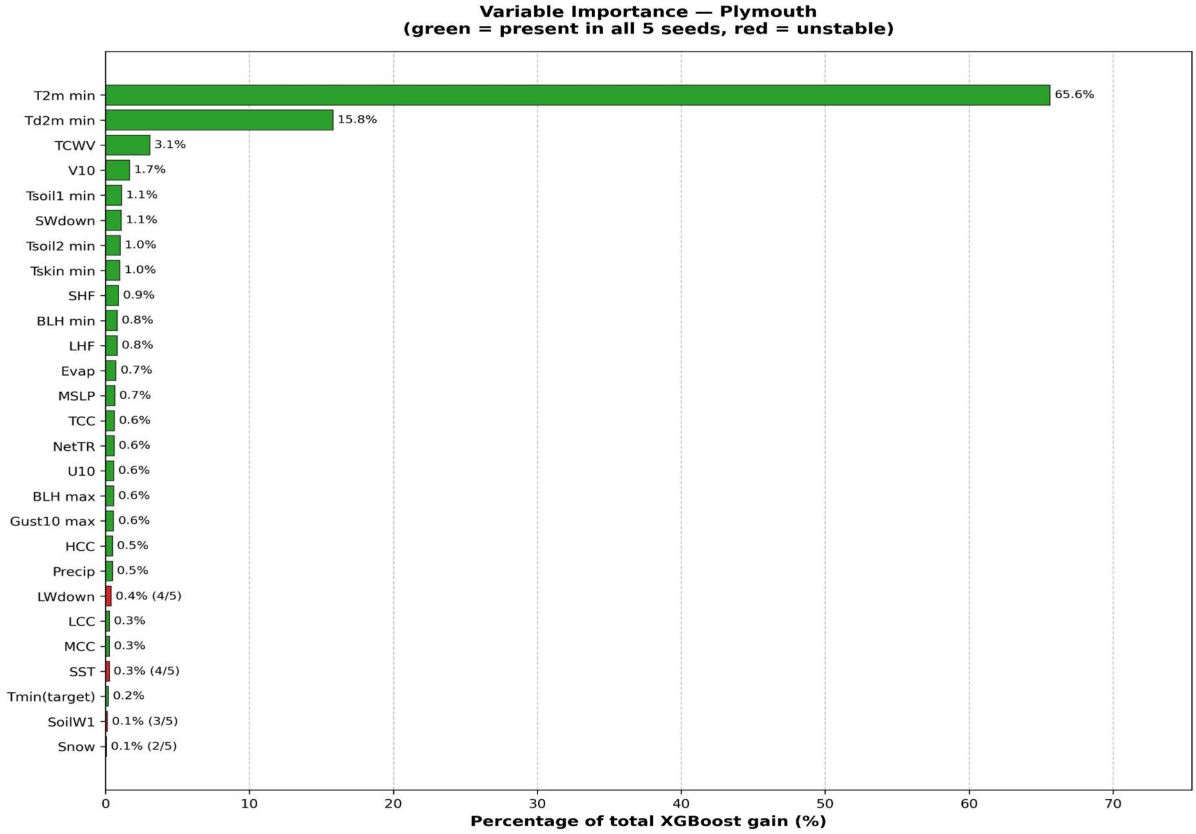

Figure 10. *Variable importance for Plymouth (oceanic climate). T2m_min strongly dominates (66%), with dewpoint temperature as distinctive oceanic signature.*

Spatial distribution

Predictor locations for Plymouth showed moderate spatial concentration, with 78% of gain within 200 km. Selected grid points were distributed across southwest England, Wales, the English Channel, and Brittany, with humidity and wind predictors preferentially located in the Atlantic sector—consistent with the dominant westerly flow that characterizes this region's climate (Wallace and Hobbs, 2006).

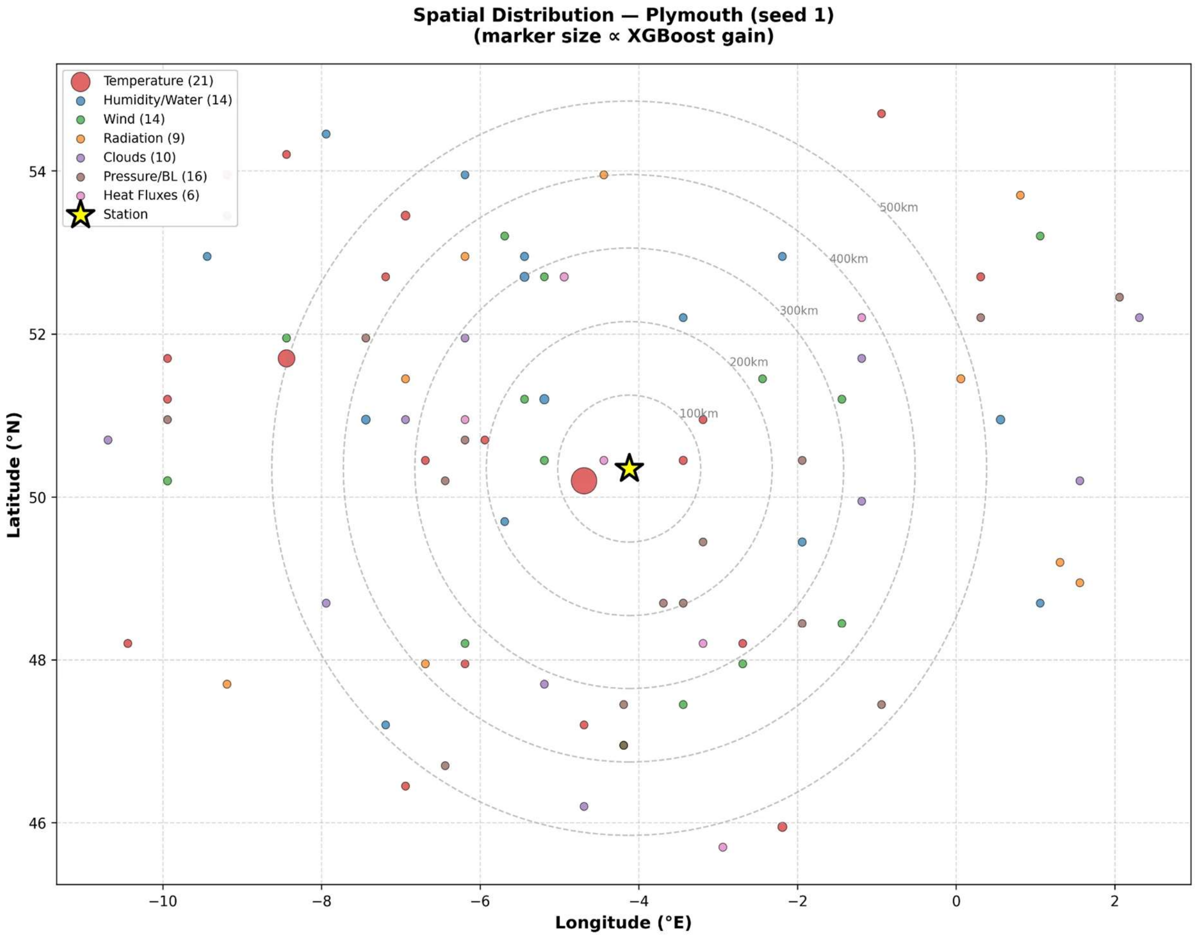

Figure 11. *Spatial distribution of selected predictors for Plymouth. Predictors extend across southwest England, Wales, and the English Channel, with humidity variables concentrated in the Atlantic sector.*

Notably, Plymouth showed degraded performance in 2024 relative to 2023 (+0.16°C increase in MAE), the largest year-to-year variation among the eight stations. This may reflect unusual meteorological conditions during the test period that warrant further investigation.

4.5 Detailed Analysis: Strasbourg (Continental Climate)

Strasbourg, located in the Upper Rhine Valley of northeastern France, exhibits a semi-continental climate with warm summers, cold winters, and large diurnal temperature ranges. This station presented the greatest prediction challenge among the three analyzed (MAE = 1.29 ± 0.02°C, R^2 = 0.93).

Variable importance

The predictor hierarchy for Strasbourg featured:

(1) *T2m_min dominated* with 65% of total gain, similar to Plymouth.

(2) *Soil temperature (layer 1)* contributed 14%—a distinctive continental signature absent from the oceanic and Mediterranean stations. This reflects the role of ground thermal inertia in modulating nocturnal cooling under the clear skies typical of continental high-pressure systems (Oke, 1987).

(3) *Skin temperature (7%)* and *total column water vapour (3%)* provided secondary contributions.

(4) *Persistence was minimal* (Tmin reference < 1%), indicating that continental climate, like oceanic climate, exhibits substantial day-to-day variability in minimum temperatures (Wilks, 2011).

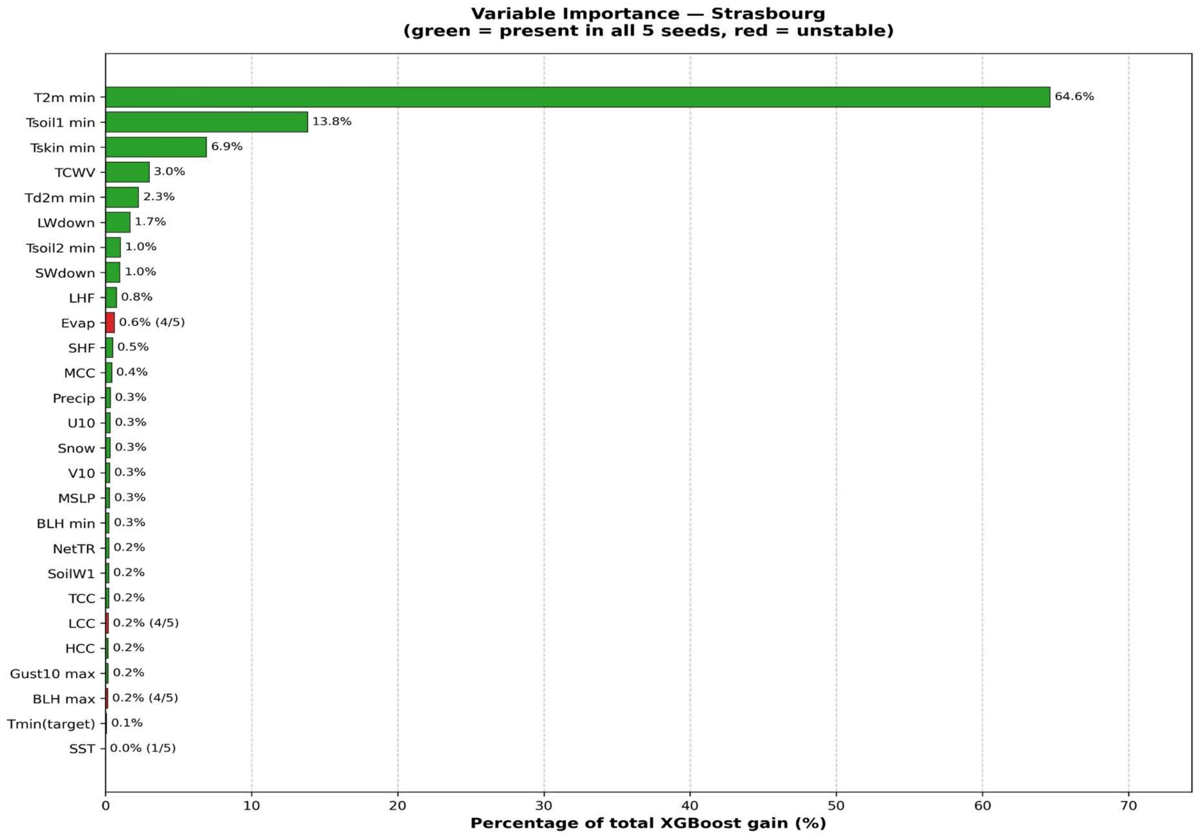

Figure 12. *Variable importance for Strasbourg (continental climate). Soil temperature (layer 1: 14%) emerges as a distinctive continental signature.*

Spatial distribution and gain concentration

Predictor locations concentrated in the Rhine Valley and surrounding regions, with 78% of gain within 200 km of the station. Some predictors were located in western France, potentially capturing the influence of Atlantic air masses that occasionally penetrate into the continental interior (Wallace and Hobbs, 2006).

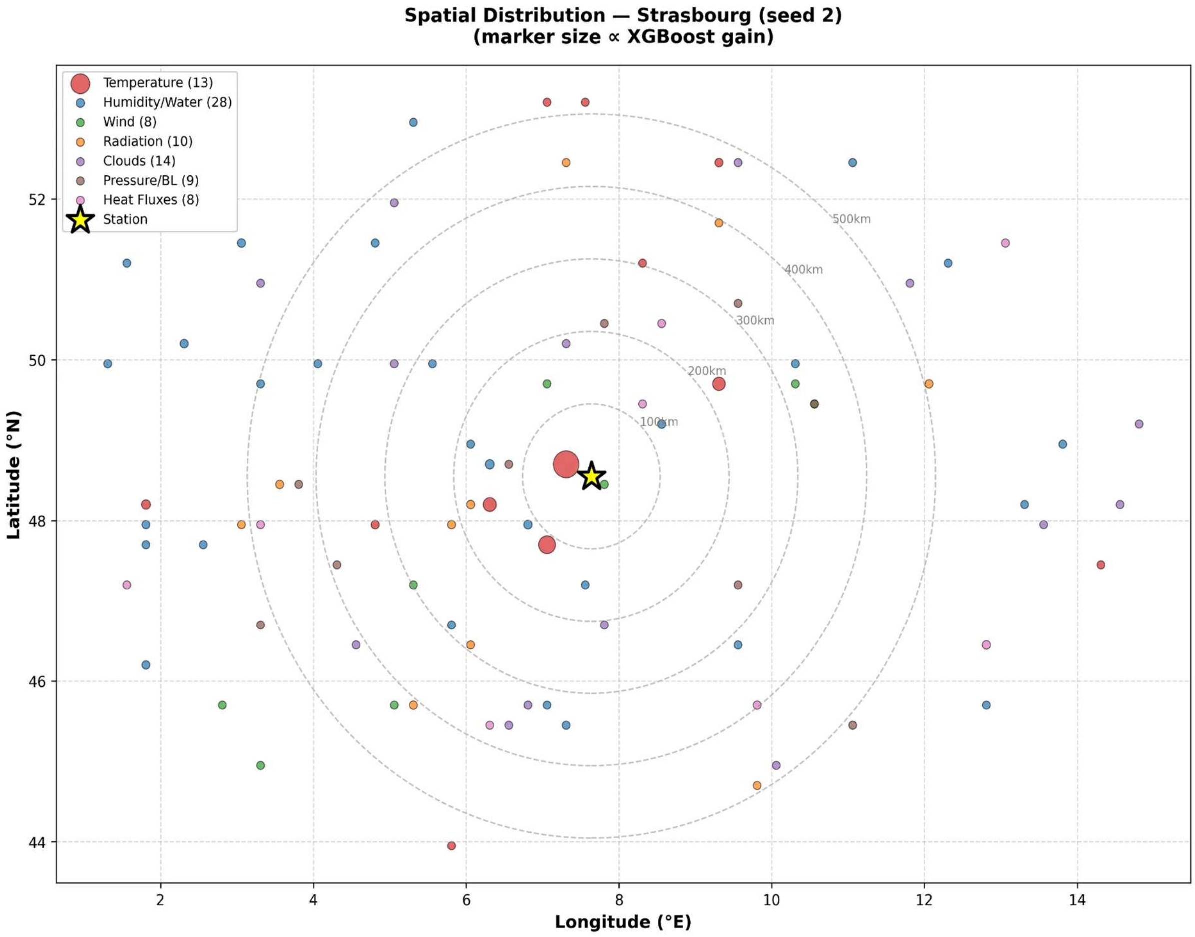

Figure 13. *Spatial distribution of selected predictors for Strasbourg. Predictors concentrate in the Rhine Valley region, with 78% of gain within 200 km of the station.*

Analysis of gain concentration revealed extreme inequality in predictor contributions: the top 4 predictors accounted for 80% of total gain, and the top 12 for 90%. The remaining 78 predictors contributed marginally, suggesting that a substantially reduced predictor set might achieve comparable performance.

Spring presented the greatest prediction challenge for Strasbourg (MAE = 1.52°C), unique among the analyzed stations. This likely reflects the transitional character of spring weather in continental climates, where rapidly shifting patterns between residual winter conditions and emerging summer regimes create high forecast uncertainty (Wallace and Hobbs, 2006).

4.6 Cross-Station Synthesis

General patterns

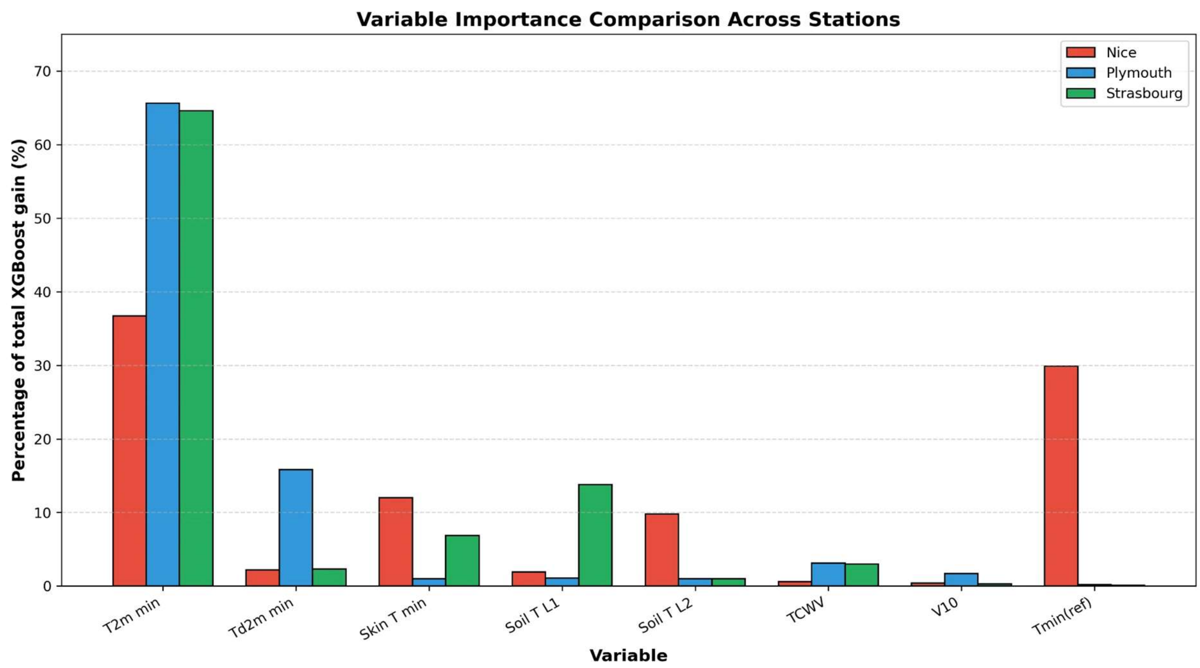

Figure 14. *Variable importance comparison across the three representative stations. T2m_min dominates at all stations (37-66%), with climate-specific secondary predictors.*

Despite substantial differences in climate and prediction difficulty, several patterns emerged consistently across all three stations:

(1) *Near-surface air temperature (T2m_min)* was universally the dominant predictor, contributing 37-66% of total gain.

(2) *The top 3 variables captured 85-90%* of total predictive information, indicating that minimum temperature forecasting is fundamentally driven by a small set of thermal variables, in line with established physical understanding of nocturnal cooling processes (Stull, 1988).

(3) *Predictive information was concentrated locally*, with 65-78% of gain originating within 200 km of each station, consistent with the spatial coherence of synoptic and mesoscale meteorological fields (von Storch and Zwiers, 1999).

(4) *Variable-level selection was highly stable* (23-24 of 26 variables present in all five independent runs), while grid-point selection showed high variability due to spatial autocorrelation, a known characteristic of gridded atmospheric data (von Storch and Zwiers, 1999).

Climate-specific signatures

Beyond these universal patterns, each climate type exhibited distinctive predictor signatures (Table 8).

Table 8. Climate-specific predictor signatures identified through the selection algorithm.

Climate	Distinctive predictor	Contribution	Physical interpretation
Mediterranean	Tmin reference	30%	Thermal stability (maritime buffer)
Oceanic	Dewpoint (Td2m)	16%	Atlantic humidity advection
Continental	Soil temperature	14%	Ground thermal inertia

These signatures align with physical understanding of each climate regime. Mediterranean climates showed strong persistence linked to maritime buffering (Oke, 1987), oceanic climates were characterized by the importance of humidity-related predictors associated with Atlantic air masses (Brutsaert, 1982), and continental climates exhibited a clear influence of soil thermal inertia (Oke, 1987). These signatures are physically consistent and reinforce the interpretability of the predictor selection methodology.

Implications for predictor selection

The extreme concentration of predictive gain (80% from top 4 predictors, 90% from top 12) suggests that the 90-predictor configuration may be over-specified for operational applications. A reduced set of 20-30 predictors, focused on thermal variables and climate-specific secondary predictors, would likely achieve comparable performance with reduced computational cost. However, retaining the broader predictor pool in the research context proved valuable for identifying the climate-specific signatures documented above.

5. Conclusion

5.1 Summary of findings

This study developed and validated an automated framework for systematic spatial exploration and predictor selection applied to next-day minimum temperature forecasting across Western Europe. By combining ERA5 reanalysis data with gradient boosting regression techniques, we identified optimal predictor configurations for eight climatically diverse reference sites, achieving substantial improvements over baseline methods.

The results demonstrate that minimum temperature forecasting benefits significantly from spatially-distributed predictors, with model performance reducing MAE by 35–54% compared to persistence and 51–64% compared to climatological means. Mediterranean climates proved easiest to predict (MAE = 0.81°C), while oceanic and continental sites presented greater challenges (MAE = 1.07–1.34°C). These performance differences reflect fundamental distinctions in the physical processes governing nocturnal cooling across climate regimes.

A key finding concerns the emergence of climate-specific predictor signatures. Mediterranean stations exhibited strong persistence signals driven by maritime thermal buffering, oceanic climates showed enhanced sensitivity to dewpoint temperature reflecting Atlantic humidity advection, and continental sites featured significant soil temperature contributions linked to ground thermal inertia. These signatures align with established meteorological understanding and demonstrate that the search algorithm successfully identifies physically meaningful predictors.

The extreme concentration of predictive gain—with 80% originating from just 4 predictors and 90% from 12—suggests that operationally efficient configurations could be derived from our comprehensive predictor analysis. The single-day temporal window proved optimal for 75% of stations tested, consistent with the principle of parsimony in time series modeling.

5.2 Broader perspectives and future applications

This work is part of a broader project aimed at leveraging time series analysis for predictive applications across multiple domains. The methodology presented here—systematic spatial exploration combined with machine learning-based predictor selection—is inherently generic and can be adapted to various forecasting challenges beyond minimum temperature prediction.

Preliminary experiments on river gauge level forecasting (e.g., the Mississippi River in St. Louis, Missouri) have yielded promising results, with the algorithm successfully identifying informative predictors using temporal window sizes larger than one day (e.g., D-3).

This application demonstrates the framework's potential for hydrological forecasting, where accurate water level predictions are essential for flood management and water resource planning. Other potential applications span diverse fields, including air quality forecasting (pollutant concentration prediction), agricultural meteorology (frost risk assessment), energy sector planning (demand forecasting), and domains entirely unrelated to Earth sciences, using dimensionalities beyond the geographic one.

While the present study used daily temporal resolution, the algorithm can be readily adapted to other time units appropriate to the problem at hand—hours for short-term operational forecasting, weeks or months for seasonal predictions, or even years for long-term trend analysis (e.g., as in seasonal forecasting frameworks discussed by Hyndman and Athanasopoulos, 2021). This temporal flexibility, combined with the spatial exploration capabilities demonstrated here, positions the framework as a versatile tool for time series prediction across scales and domains, aligning with broader applications of machine learning in environmental sciences (Reichstein et al., 2019).

5.3 Operational considerations

While the predictor selection algorithm explores a vast search space (~45,000 candidates) to identify the optimal 90-predictor set per site, it is designed for infrequent execution—typically once per year or every two years—to incorporate newly available data and maintain relevance under evolving climate conditions. This process requires approximately one hour of computation per site on a standard personal computer, making it feasible for periodic updates without significant resource demands.

In contrast, daily forecasting operations leverage the pre-selected predictor set: the XGBoost regression model is applied using current-day values from these 90 predictors, completing inference in mere tens of seconds. This separation between offline optimization (guided by MAE as a directional metric) and online prediction ensures scalability and efficiency, allowing the framework to be deployed in real-time systems while focusing primarily on discovering robust, physically meaningful predictor configurations rather than minimizing absolute error in isolation, as emphasized in operational ML guidelines (Sculley et al., 2015).

References

Bergmeir, C. and Benitez, J. M.: On the use of cross-validation for time series predictor evaluation, Information Sciences, 191, 192-213, https://doi.org/10.1016/j.ins.2011.12.028, 2012.

Box, G. E. P. and Jenkins, G. M.: Time Series Analysis: Forecasting and Control, Holden-Day, San Francisco, CA, USA, 1976.

Box, G. E. P., Jenkins, G. M., Reinsel, G. C., and Ljung, G. M.: Time Series Analysis: Forecasting and Control, 5th edn., Wiley, Hoboken, NJ, USA, 2015.

Brutsaert, W.: Evaporation into the Atmosphere: Theory, History, and Applications, Springer, Dordrecht, the Netherlands, https://doi.org/10.1007/978-94-017-1497-6, 1982.

Burnham, K. P. and Anderson, D. R.: Model Selection and Multimodel Inference: A Practical Information-Theoretic Approach, 2nd edn., Springer, New York, NY, USA, https://doi.org/10.1007/b97636, 2002.

Chen, T. and Guestrin, C.: XGBoost: A scalable tree boosting system, Proceedings of the 22nd ACM SIGKDD International Conference on Knowledge Discovery and Data Mining, San Francisco, CA, USA, 785-794, https://doi.org/10.1145/2939672.2939785, 2016.

Glahn, H. R. and Lowry, D. A.: The use of Model Output Statistics (MOS) in objective weather forecasting, J. Appl. Meteorol., 11, 1203-1211, https://doi.org/10.1175/1520-0450(1972)011<1203:TUOMOS>2.0.CO;2, 1972.

Hersbach, H., Bell, B., Berrisford, P., Hirahara, S., Horanyi, A., Munoz-Sabater, J., Nicolas, J., Peubey, C., Radu, R., Schepers, D., Simmons, A., Soci, C., Abdalla, S., Abellan, X., Balsamo, G., Bechtold, P., Biavati, G., Bidlot, J., Bonavita, M., De Chiara, G., Dahlgren, P., Dee, D., Diamantakis, M., Dragani, R., Flemming, J., Forbes, R., Fuentes, M., Geer, A., Haimberger, L., Healy, S., Hogan, R. J., Holm, E., Janiskova, M., Keeley, S., Laloyaux, P., Lopez, P., Lupu, C., Radnoti, G., de Rosnay, P., Rozum, I., Vamborg, F., Villaume, S., and Thepaut, J.-N.: The ERA5 global reanalysis, Q. J. Roy. Meteor. Soc., 146, 1999-2049, https://doi.org/10.1002/qj.3803, 2020.

Holmberg, S., Messori, G., Caballero, R., and Faranda, D.: Forecasting atmospheric persistence and implications for the predictability of temperature and temperature extremes, Q. J. Roy. Meteor. Soc., https://doi.org/10.1002/qj.4885, 2024.

Hyndman, R. J. and Athanasopoulos, G.: Forecasting: Principles and Practice, 3rd edn., OTexts, Melbourne, Australia, available at: https://otexts.com/fpp3/ (last access: 3 January 2026), 2021.

Jolliffe, I. T. and Stephenson, D. B. (Eds.): Forecast Verification: A Practitioners Guide in Atmospheric Science, 2nd edn., Wiley, Chichester, UK, https://doi.org/10.1002/9781119960003, 2012.

Ke, G., Meng, Q., Finley, T., Wang, T., Chen, W., Ma, W., Ye, Q., and Liu, T.-Y.: LightGBM: A highly efficient gradient boosting decision tree, Advances in Neural Information Processing Systems, 30, 3146-3154, 2017.

Lakshmanan, V., Gronemeijer, E., McGovern, A., and Elmore, K.: Machine Learning and Data Mining Approaches to Climate Science, Springer, Cham, Switzerland, https://doi.org/10.1007/978-3-319-17220-0, 2015.

Menne, M. J., Durre, I., Vose, R. S., Gleason, B. E., and Houston, T. G.: An overview of the Global Historical Climatology Network-Daily database, J. Atmos. Ocean. Tech., 29, 897-910, https://doi.org/10.1175/JTECH-D-11-00103.1, 2012.

Oke, T. R.: Boundary Layer Climates, 2nd edn., Routledge, London, UK, https://doi.org/10.4324/9780203407219, 1987.

Peel, M. C., Finlayson, B. L., and McMahon, T. A.: Updated world map of the Koppen-Geiger climate classification, Hydrol. Earth Syst. Sci., 11, 1633-1644, https://doi.org/10.5194/hess-11-1633-2007, 2007.

Prechelt, L.: Early stopping - but when?, in: Neural Networks: Tricks of the Trade, edited by: Orr, G. B. and Muller, K.-R., Lecture Notes in Computer Science, vol. 1524, Springer, Berlin, Heidelberg, Germany, 55-69, https://doi.org/10.1007/3-540-49430-8_3, 1998.

Reichstein, M., Camps-Valls, G., Stevens, B., Jung, M., Denzler, J., Carvalhais, N., and Prabhat: Deep learning and process understanding for data-driven Earth system science, Nature, 566, 195-204, https://doi.org/10.1038/s41586-019-0912-1, 2019.

Sculley, D., Holt, G., Golovin, D., Davydov, E., Phillips, T., Ebner, D., Chaudhary, V., Young, M., Crespo, J.-F., and Dennison, D.: Hidden technical debt in machine learning systems, Advances in Neural Information Processing Systems, 28, 2503-2511, 2015.

Stull, R. B.: An Introduction to Boundary Layer Meteorology, Kluwer Academic Publishers, Dordrecht, the Netherlands, https://doi.org/10.1007/978-94-009-3027-8, 1988.

von Storch, H. and Zwiers, F. W.: Statistical Analysis in Climate Research, Cambridge University Press, Cambridge, UK, https://doi.org/10.1017/CBO9780511612336, 1999.

Wallace, J. M. and Hobbs, P. V.: Atmospheric Science: An Introductory Survey, 2nd edn., Academic Press, Amsterdam, the Netherlands, https://doi.org/10.1016/C2009-0-00034-8, 2006.

Wilks, D. S.: Statistical Methods in the Atmospheric Sciences, 3rd edn., Academic Press, Amsterdam, the Netherlands, https://doi.org/10.1016/C2017-0-03921-6, 2011.

Willmott, C. J. and Matsuura, K.: Advantages of the mean absolute error (MAE) over the root mean square error (RMSE) in assessing average model performance, Clim. Res., 30, 79-82, https://doi.org/10.3354/cr030079, 2005.

Xue, B., Zhang, M., Browne, W. N., and Yao, X.: A survey on evolutionary computation approaches to feature selection, IEEE T. Evolut. Comput., 20, 606-626, https://doi.org/10.1109/TEVC.2015.2504420, 2016.

Code availability

All code developed for this study—including the predictor selection algorithm, data processing pipelines, analysis scripts, model training configurations, and results files (json)—will be made publicly available upon publication via repositories such as GitHub and Zenodo, with a permanent DOI assigned to the archive. The exact links will be provided upon request. A Cython-compiled high-performance version of the selection algorithm will also be provided. Docker container ensuring full reproducibility of the computational environment will be released alongside the code repository. This repository will be publicly released within 8 to 10 weeks of this preprint.

Data availability

ERA5 reanalysis data are freely available from the Copernicus Climate Data Store (https://cds.climate.copernicus.eu). Daily minimum temperature observations were obtained from NOAA's National Centers for Environmental Information Global Summary of the Day dataset (https://www.ncei.noaa.gov).

Author contribution

Eric Duhamel designed the study, developed the methodology, wrote the code, performed the analyses, and prepared the manuscript.

Competing interests

The author declares that there is no conflict of interest.

Acknowledgements

This work was conducted independently without institutional affiliation. The author thanks the European Centre for Medium-Range Weather Forecasts (ECMWF) for providing open access to ERA5 reanalysis data through the Copernicus Climate Change Service, and NOAA's National Centers for Environmental Information (NCEI) for maintaining and distributing the station observation records used in this study. The author welcomes inquiries from researchers or institutions interested in collaboration or in applying this methodology to other forecasting challenges.

Financial support

This research received no external funding.